Antibacterial properties of silver nanoparticles grown *in situ* and anchored to titanium dioxide nanotubes on titanium implant against *Staphylococcus aureus*

Urvashi F. Gunputh [1, 2], Huirong Le [2*], Kiruthika Natesan[3], Alexandros Besinis [1], Christopher Tredwin [3] and Richard D. Handy [4*]

[1]*School of Engineering, Plymouth University, Plymouth, PL4 8AA, United Kingdom*

[2]*School of Mechanical Engineering and Built Environment, University of Derby, DE22 3AW, United Kingdom*

[3]*Peninsula Schools of Medicine and Dentistry, Plymouth University, Research Way, Plymouth, Devon, PL6 8BU, United Kingdom*

[4]*School of Biological & Marine Sciences, Plymouth University, PL4 8AA, United Kingdom*

Corresponding Authors: r.handy@plymouth.ac.uk (R. D. Handy) and h.le@derby.ac.uk (H. R. Le).

Abstract

Medical grade titanium alloy, Ti-6Al-4V, with TiO_2 nanotubes (TiO_2-NTs) grown on the surface and then decorated with silver nanoparticles (Ag NPs) is proposed to enhance the antimicrobial properties of the bone/dental implants. However, the decoration with Ag NPs is not consistent and there are concerns about the direct contact of Ag NPs with human tissue. The aim of this study was to achieve a more even coverage of Ag NPs on TiO_2-NTs and determine their biocidal properties against *Staphylococcus aureus*, with and without a top coat of nano hydroxyapatite (nHA). The decoration with Ag NPs was optimised by adjusting the incubation time of the TiO_2-NTs in a silver ammonia solution, and using biocompatible δ-gluconolactone as a reducing agent. The optimum incubation in silver ammonia was 7 minutes, and resulted in evenly distributed Ag NPs with an average diameter of 47.5 ± 1.7 nm attached to the surface of the nanotubes. The addition of nHA did not compromise the antimicrobial properties of the materials; high resolution electron microscopy showed *S. aureus* did not grow on the composite with nHA and with >80 % biocidal activity measured by the LIVE/DEAD assay, also limited lactate production. Dialysis experiment confirmed the stability of the coatings, and showed a slow release of dissolved silver (3.27 ± 0.15 μg/L over 24 h) through the top coat of nHA.

Keywords: Silver nanoparticles, titanium dioxide nanotubes, nano hydroxyapatite, *Staphylococcus aureus*, antimicrobial, silver dissolution

Introduction

Orthopaedic and dental implants should be suitably durable with mechanical properties that mimic the intended tissue (O'Brien, 2011). The implants must also be biocompatible and ideally exhibit some antimicrobial properties as infection post-surgery is an underlying cause of implant failure (Connaughton *et al.,* 2014). The challenge is to make a medical implant with all these attributes. Titanium dioxide nanotubes (TiO_2-NTs) are readily grown on medical grade titanium whereby they can resist mechanical stresses similar to those faced by bone (Descamps *et al.,* 2013). They have also been shown to be biocompatible with bone cells, partly because they mimic the surface morphology of bone (Brammer *et al.,* 2012). Crucially the properties of TiO_2-NTs can be tuned to the clinical application by varying the thickness, surface texture and/or decoration of the nanotubes (Spriano *et al.*, 2018). The relationship between the surface properties of TiO_2-NTs and mechanistic responses of osteoblast cells is also partially understood (Meyerink *et al.*, 2018). However, TiO_2-NTs alone are not antimicrobial (Zhao *et al*., 2011).

Staphylococcus aureus is one of the most common cause of infection in implants (Rodríguez-Cano *et al.*, 2014). To enhance antimicrobial properties, TiO_2-NTs can be coated with antibiotics such as gentamicin (Yang *et al.*, 2016) or vancomycin (Zhang *et al.*, 2013). However, infections related to implants are normally caused by a mixture of microbes (Nie *et al.*, 2017) and individual antibiotics are inevitably only targeted at a few of the organisms present. There is also the concern of antibiotic resistance (Moriarty *et al.*, 2016). Alternatively, dissolved metals such as silver, copper and zinc have been known for their antimicrobial properties for centuries. Their solubility and biological reactivity have restricted their applications to simple disinfectants in the past, but now nanoparticulate forms of these metals are available. Of these metals, silver nanoparticles (Ag NPs, review, Reidy *et al*., 2013) are arguably the strongest biocide with minimum

inhibitory concentrations (MIC) for growth of 3.25 mg/l to *S. mutans* (Besinis *et al*., 2014a). Ag NPs are also toxic to *S. sanguinus* when presented as a silver coating on medical grade titanium alloy (Besinis *et al*., 2017). However, the rapid release of Ag from silver-containing coatings may cause toxicity to mammalian cells (Gao *et al.*, 2014), and instead a controlled release of Ag by enhancing the stability of the coating is desirable (Zhao *et al.*, 2011).

It is also possible to decorate Ag NPs onto the surface of TiO_2-NTs using anodization methods (Gunputh *et al.*, 2018), and then add another biocompatible material to control the Ag release. TiO_2-NTs can also be decorated with Ag NPs in the presence of calcium phosphate NPs (Chernozem *et al.*, 2019), but there are some concerns about the elastic properties and nanohardness of the implant material when $Ca_3(PO_4)_2$ is used (Chernozem *et al.*, 2017). One possible alternative approach is to 'top-coat' the silver-containing nanomaterial with a layer of biocompatible hydroxyapatite (HA), so that there is no hazard to the human tissue and better mechanical properties. Hydroxyapatite (HA) has a similar structure to bone and is well-known as a biocompatible material that promotes osteointegration (Ramires *et al.*, 2001, Balani *et al.*, 2007). Nano forms of HA (nHA) are also available (Ha *et al.*, 2015). Our previous work developed an anti-bacterial coating consisting of TiO_2-NTs grown on Ti-6Al-4V alloy, with clusters of Ag NPs on the TIO_2-NT surface (Gunputh *et al.*, 2018). The aim of the present study was to develop these coatings further by optimising the incubation time with reducing agents to provide a more uniform decoration of Ag NPs, and crucially, to determine if antibacterial properties remained after top coating the materials with nHA. To demonstrate the antimicrobial properties, the final composite coatings were tested against *S. aureus*. For these latter studies, this included counting the proportions of live and dead bacteria on the

coatings, monitoring microbial activity with a lactate production assay, as well as electron microscopy to observe coating integrity and the presence of any microbes.

Materials and Method

Titanium dioxide nanotubes (TiO_2-NTs) were self-assembled on the surface of Ti-6Al-4V alloy discs followed by the chemical reduction of silver to form Ag NPs on the nanotubes. For some of the silver coated nanotubes, nHA was sintered to the composite coating. After characterising the different coatings formed, the antibacterial properties of all of them were tested in the presence of *S. aureus*.

Growth of TiO_2-NTs with Ag NPs and HA coating

The synthesis of the composite coatings started with TiO_2-NTs followed by the addition of Ag NPs and last nHA. To start with, the self-assembly of the TiO_2-NTs on to titanium alloy discs was conducted using an anodisation process as previously optimised (Danookdharree *et al.*, 2015). Briefly, this was a 1 hour electrochemical reaction in a mixture of 1 mol/L NH_4HPO_4 and 0.5 wt% NH_4F (0.5 g of NH_4F in 100 mL of ammonia solution) at 20 V. All the coated discs were then annealed at 350 ºC for 2 h in a furnace to achieve the anatase phase (Carbolite RWF 1200, Carbolite Engineering Services, Hope Valley, UK). The TiO_2-NTs were then functionalised by treating them with 2 mol/L NaOH at 50 ºC for 2 minutes (Parcharoen *et al.*, 2014). This resulted in the formation of sodium titanate ($Na_2Ti_3O_7$) which is a reactive surface for the next steps in the synthesis of the composite material.

Silver nanoparticles were then chemically reduced on the surface of the TiO_2-NTs as previously described (Gunputh *et al.*, 2018). Briefly, a silver ammonia solution was prepared, at room temperature and with continuous stirring, by mixing 2.545 g of silver nitrate and 900 mL of ultrapure water, followed by 15 mL of 1 M NaOH. A precipitate

of silver oxide formed, but was continuously mixed to remain in suspension. Concentrated liquid ammonia (13.4 M; density, 0.910 kg/m^3) was then added dropwise to the mixture until all the oxide had dissolved. Pure water was then added to bring the final volume to 1000 mL. The resulting solution of silver ammonia, $[Ag(NH_3)_2]^+$, (15 mM) was allowed to stir for a further 10 minutes to ensure complete reaction and mixing. Afterwards, 2 mM δ-gluconolactone solution (Sigma Aldrich, UK) was prepared in 12 mM NaOH, the volume of which was dependent on the experiment performed.

The titanium alloy discs covered with TiO_2-NTs were immersed in silver ammonia first, allowing the cationic silver ammonia to attach to $–O^-$ residues of the nanotubes (Gunputh *et al.*, 2018). After an initial exposure to the silver ammonia, the samples were ultrasonicated in deionised water at 12 MHz for 5 minutes to remove any loosely attached silver ammonia; after which the disks were air dried at room temperature. The samples were then exposed to the gluconolactone solution for 5 minutes. Depending on the exposure time to silver ammonia, the samples were identified as TiO_2-Ag3, TiO_2-Ag7 and TiO_2-Ag10 for an exposure of 3, 7 and 10 minutes in silver ammonia respectively, and all treated for 5 minutes in gluconolactone solution (n = 3 each). Gluconolactone was expected to reduce the silver ammonia to Ag NPs which are attached on the surface of the TiO_2-NTs. The samples were again ultrasonicated in deionised water for 5 minutes with the aim of removing the loosely attached Ag NPs.

After the optimisation of the incubation time for the synthesis of Ag NPs on the TiO_2-NT discs, hydroxyapatite was finally added using a sintering method (Besinis *et al.*, 2017). Briefly, 7 minutes was deemed the optimum time for the silver ammonia treatment, and so TiO_2-Ag7 discs were placed in 24-well plates and sterilised with 70 % ethanol (n = 12 discs). Afterwards, 20 µL of 10 wt% nHA solution (Sigma Aldrich, UK) was evenly pipetted on top of the discs after which they were left to dry at room

144 temperature for 48 hours. Subsequently, the discs were placed in a porcelain dish and
145 gradually heated (Carbolite furnace, Hope, UK) at 10 °C per min to 500 °C. The final
146 temperature was maintained for 10 minutes after which the temperature was gradually
147 reduced to room temperature. The 500 °C temperature was chosen as it was high enough
148 to cause sintering, while being below the melting point of silver. The change in
149 temperature was gradual to ensure maintaining the crystallinity of the nHA. The resulting
150 discs are hereafter termed 'TiO_2-Ag7-HA'.
151
152 ***Characterisation of the coatings***
153 The morphology and chemical composition of the TiO_2 at each step of the synthesis (i.e.,
154 addition of Ag-NPs and then HA) was analysed by scanning electron microscopy with
155 energy dispersive spectroscopy (SEM/EDS). Figure 1 shows the surface morphology
156 prior to the HA additions and for different incubations times with silver ammonia. The
157 growth of the TiO_2-NTs gave generally good coverage of the alloy, as expected
158 (Danookdharree *et al.*, 2015). When 3 minutes incubation time was used (TiO_2-Ag3), the
159 TiO_2-NTs had less spherical Ag NPs on the surface (Figure 1B). The samples incubated
160 for 7 minutes (TiO_2-Ag7) had a more uniform distribution of Ag NPs. In both TiO_2-Ag3
161 and TiO_2-Ag7, the nanotubular characteristic of the TiO_2 was still visible after the growth
162 of Ag NPs. However in TiO_2-Ag10, the Ag NPs grown covered the whole surface of the
163 TiO_2 with some clustering observed (Figure 1D). The EDS analysis of the white spherical
164 nanoparticles on the discs confirmed the presence of silver with the weight percentage of
165 the latter over the coating increasing from TiO_2-Ag3 to TiO_2-Ag10 (5-8 wt%) to the
166 contrary of Ti, Al and O which were found to be decreasing. The incubation time also
167 affected the primary size of the Ag NPs, as observed by electron microscopy, with
168 diameters of 88.25 ± 5.1, 47.5 ± 1.7, 30 ± 2.4 nm for incubations of 3, 7 and 10 minutes

169 with silver ammonia, respectively (all significantly different from each other, ANOVA,
170 $P < 0.05$).

171 For the logistics of biological testing, one 'best' composite had to be selected for
172 experimental work. After considering all the characterisation information, TiO_2-Ag7 was
173 chosen as the coated samples to be taken forward for further testing. This was selected on
174 the basis that it had the most uniform coating with almost no clustering of and full surface
175 coverage of the Ag NPs (Figure 2). After the addition of nHA to the latter coating, another
176 uniformly distributed coating was obtained (Figure 2B). The EDS analysis (Figure 2D)
177 confirms the presence of Ca and P as part of the nHA. As expected, the amount of silver
178 now detected with the HA surface was less than TiO_2-Ag7 alone (< 5 wt %). Some
179 cracking of the nHA layer was observed (Figure 2D), but this regarded as a desirable
180 feature to facilitate the slow release of the underlying silver.

181

182 ***Dialysis experiment and the release of dissolved metal***

183 A dialysis experiment was conducted according to Besinis *et al* (2014b) using the TiO_2-
184 Ag7 and TiO_2-Ag7-HA discs to inform on the release of any dissolved Ag with respect
185 to antibacterial properties, and on the stability of the coatings (Besinis *et al.*, 2014a). A
186 simulated body fluid (SBF) was used for these experiments (in mmol/l): Na^+, 142; K^+,
187 5.0; Mg^{2+}, 1.5; Ca^{2+}, 2.5; Cl^-, 147.8; HCO_3^-, 4.2; HPO_4^{2-}, 1.0; SO_4^{2-}, 0.5 (Kokubo *et al.*,
188 1990), with the pH adjusted to 7.2 with a few drops of 1 mol/L HCl. Experiments were
189 conducted in triplicate at room temperature in previously acid washed (5% nitric acid)
190 and deionised glassware. Dialysis tubing (MW cut off, 12 000 Da, Sigma Aldrich, UK),
191 was cut in 7 cm x 2.5 cm lengths and sealed at one end using a Mediclip; then filled with
192 one Ti alloy discs as appropriate with 7 mL of SBF. The dialysis bag was closed with
193 another Mediclip and then suspended in a 500 mL pyrex glass beaker containing 243 mL

of SBF (i.e., total volume 250 mL). The beakers were gently stirred throughout, and 4 mL aliquots of the SBF were collected from the external compartment of the beaker at 0, 0.5, 1, 2, 3, 4, 6, 8, 24 h. The SBF samples were acidified with a drop of 70 wt% nitric acid and stored for metal analysis (see below). At the end of the 24 h, the dialysis bags were also carefully opened and 4 ml of the fluid therein collected for metal analysis. Dialysis curves were plotted using SigmaPlot 13.0 (Systat Software, Inc.), after deducting the background ionic concentrations of the SBF. A first order rectangular hyperbola function was used to fit dialysis curves to the raw data. The maximum initial slope of the curves informed on the maximum apparent dissolution rate of each substance.

Plate preparation and exposure to S. aureus

The experimental design involved exposing *S. aureus* to the coated samples of TiO_2-Ag7 and TiO_2-Ag7-HA in 24-well, flat-bottom sterile polystyrene plates (Thermo Fischer Scientific, Loughborough, UK). TiO_2-NT coated discs were used as a control for the composite coating effect. Silver nitrate was used as a metal salt control for any possible dissolved silver effect from the coating. Silver nanoparticles alone were also used as a control for Ag NP effect that might arise from the coatings. *S. aureus* was allowed to grow on its own as a negative control. Nine replicate runs were conducted for each type of coated samples and the controls (n = 6 for biochemical assays and n = 3 for SEM). Following the approach by Besinis *et al* (2014a), the materials were exposed to *S. aureus* for 24 h and the proportion of live to dead cells and the amount of lactate produced were evaluated (see biochemical assays below). The concentration of total dissolved silver, calcium and phosphorus released from the coating in the SBF were also measured.

S. aureus was chosen as it is considered to be one of the main causes of infection in orthopaedic and dental implants (Swank and Dragoo, 2013, Tsikandylakis *et al.*, 2014).

S. aureus was cultured in brain heart infusion (BHI) broth (Lab M Ltd, Bury, UK) at 37 ºC. A bacterial suspension having optical density 0.018 at 595 nm absorbance (Spectrophotometer Genesys 20, Fisher Scientific, Loughorough, UK) was prepared in the BHI broth at a concentration of 1×10^7 cells/mL. For the experiments, 2 mL of the bacterial culture was pipetted in each well of a 24-well plate containing TiO_2-NTs, TiO_2-Ag7, TiO_2-Ag7-HA, $AgNO_3$ (0.001M), or Ag NPs (107.9 mg/L equal to 0.001M) dispersed in ultrapure deionised water on their own (n = 9 replicates of each). A silver concentration of 0.001M was used for the positive controls as it was found that 0.001M was the maximum amount of silver released from the coatings. The 24-well microplates were then incubated at 37 ºC on a shaking table. At the end of the overnight exposure, six of the replicate plates were used for biochemistry. An aliquot (1 mL) of the exposed broth from each well were collected for the LIVE/DEAD® kit and lactate production assays (see below). The remaining broth was acidified with 70 wt% HNO_3 and used for metal determination. Then the remaining adherent bacterial were collected. Bacterial pellets were obtained whereby the samples from the wells were sonicated (12 MHz) for 60 s in 2 mL of sterile saline to remove the bacteria from the discs (Besinis *et al.*, 2014b). Then, 1 mL of the resulting suspension were allowed to grow in 5 mL of BHI broth for 5 h at 37 ºC on a shaking table with the aim of increasing the amount of live cells in order to readily measure them with the Live/Dead assay. The viability of the cells and the amount of lactate in the suspension was also assessed, followed by the measurement of the ionic composition of the latter. For the remaining three replicates, the broth was removed and the samples were prepared for electron microscopy.

Cell viability and lactate production assays

The cell viability of *S. aureus* in both the exposed broth and incubated cell suspension from all of the relevant treatments and controls [TiO_2-NTs, TiO_2-Ag7, TiO_2-Ag7-HA, $AgNO_3$ (0.001M), and Ag NPs] were assessed using the L7012 LIVE/DEAD® Backlight™ Kit (Invitrogen Ltd, Paisley, UK), exactly according to Gunputh *et al*. (2018). Briefly, 100 µL of the exposed broth and 100 µL of the incubated homogenate from each replicate was subject to several washes with sterile NaCl solution. Then 100 µL of the final suspension from each well were used for fluorimetry in clean 96 well plates with 100 µL of freshly prepared dyes from the LIVE/DEAD kit. Microplate were incubated in the dark at room temperature for 15 min and the fluorescence measured on a Cytofluor II fluorescence plate reader (excitation, 485 nm; emission at 530 nm and 645 nm). The readings at 530 nm were divided by the readings at 645 nm in order to obtain the percentage of live to dead cells in the exposed broth and the incubated cell suspension from the different samples and controls according to the kit instructions.

The metabolic activity of *S. aureus* was assessed by measuring the amount of lactate present in both the exposed broth and incubated cell suspension from the wells containing TiO_2-NTs, TiO_2-Ag7, TiO_2-Ag7-HA, $AgNO_3$ (0.001M), and Ag NP (6 replicates of each) according to Besinis *et al* (2013). Briefly, 100 µL of the exposed broth, or 100 µL of the incubated homogenate as appropriate, were transferred to a V-bottom 96-well microplate and were centrifuged at 2000 rpm for 10 minutes to generate a clean supernatant that could be measured for total lactate. Then, in a new plate, 1 µL of 1000 units/mL of lactate dehydrogenase (Sigma-Aldrich Ltd, UK) was pipetted into wells of a 96-well plate followed by 10 µL of 40 mmol/L nicotinamide adenine dinucleotide and 200 µL of 0.4 mol/L hydrazine prepared in a glycine buffer of pH 9. Ten µL of the supernatants were then added, mixed and incubator at 37ºC for 2 hours to allow lactate production to occur.

The absorbance was then read at 340 nm against lactic acid as standards (0, 0.25, 0.5, 1.0, 2.0, 4.0, 8.0 mmol/L).

Metal analysis following S. aureus exposure

The exposed broth and the detached bacteria were analysed for silver, calcium and phosphorus composition. After the exposure to *S. aureus*, 1 mL of the broth or the detached bacteria were diluted with Milli-Q water to a final volume of 5 mL and acidified (few drops of 70 wt% nitric acid). Total Ag concentrations were determined by inductively coupled plasma mass spectrometry (ICP-MS, Varian 725-ES Melbourne, Australia), and total Ca or P by optical emission spectrometry (ICP-OES, Thermo Scientific XSeries 2, Hemel Hempstead, UK). Calibrations for both instruments were performed with matrix-matched analytical grade standards. For ICP-MS the standards and samples contained internal references (0.5, 0.25 and 1% of iridium) for SBF, broth and any homogenates made from bacteria. In the complex matrix of broth and SBF, the detection limit was around 0.001 µg/L for Ag by ICP-MS, and 5 µg/L for Ca and 40 µg/L for P by ICP-OES.

Imaging of the attached S. aureus

The remaining 3 repeats of the control, TiO_2, TiO_2-Ag7, TiO_2-Ag7-HA, $AgNO_3$ and Ag NP were examined by scanning electron microscope to confirm the presence of *S. aureus* on the different surfaces. After the 24 h exposure to *S. aureus*, the supernatants were removed and the plates carefully washed twice with sterile saline (0.85 wt% NaCl). Then 2 mL of 3 wt% glutaraldehyde in 0.1 mol/L cacodylate buffer was added to each well and was allowed to stay overnight at 4 ºC. The next day, the glutaraldehyde was removed and the samples were washed with 0.1 mol/L cacodylate buffer. Specimens were serially

dehydrated through ethanol solutions, coated with carbon, and viewed under a JEOL7001F SEM. Each specimen was viewed at three different random locations (i.e., 3 images of each specimen x 3 replicate samples). Care was taken to systematically photograph the specimens without bias and at the same magnifications for all treatments.

Statistical analysis

The data from the cell viability assay, the lactate production assay and the ionic concentration measurements were analysed using Statgraphics Centurion XVII (StatPoint Technologies, Inc.). After descriptive statistics, data were checked for normality and for equal variances (Levene's test). When data were parametric, the data was analysed for treatment or time effects using one way ANOVA with Fisher's LSD test post-hoc. In cases of unequal variances, the data were transformed before analysis and where the data remained non-parametric, the Kruskal Wallis test was used. Data are presented as mean ± S.E.M unless otherwise stated. The default 95% confidence level was used for all statistics.

Results

Dialysis experiment and the stability of coatings

Figure 3 shows the results of the dialysis experiments. The total concentration of silver from the samples without any silver coatings was minimal as expected. In the presence of Ag-containing materials, there was a rise in the total Ag concentration in the external compartment of the dialysis bag, reaching a maximum of 5.44 ± 0.06 and 3.27 ± 0.15 µg/L from TiO_2-Ag7 and TiO_2-Ag7-HA respectively. The maximum dissolution rates were 0.17 ± 0.01 µg/h and 0.21 ± 0.05 µg/h for Ag from TiO_2-Ag7 and TiO_2-Ag7-HA respectively (statistically different, ANOVA, $p<0.05$, $n = 3$). Figure 3 also shows the

316 dissolution of calcium and phosphorus from the coated samples. A similar trend in the
317 total concentration was observed for both Ca and P in the beaker (Figure 3B and 3C). The
318 maximum concentration of Ca reached was 86.5 ± 1.48 and 92.0 ± 0.36 mg/L from TiO_2-
319 Ag7 and TiO_2-Ag7-HA respectively with a maximum dissolution rate of 68.8 ± 1.92 mg/h
320 and 73.4 ± 0.07 mg/h respectively. The maximum concentration of P reached was 27.6 ±
321 0.73 and 28.4 ± 0.24 mg/L from TiO_2-Ag7 and TiO_2-Ag7-HA respectively with a
322 maximum dissolution rate of 21.8 ± 0.42 and 23.0 ± 0.51 mg/h respectively.

323 ***Confirming silver exposure in the broth during S. aureus exposures***

324 The measured total Ag concentrations in the broth during the exposure of *S. aureus* to the
325 different composite coating and relevant controls are shown in Figure 4A. For the controls
326 and materials without silver, as expected they showed only a background concentration
327 of the metal (6.78 μg/L). The positive controls of $AgNO_3$ and Ag NPs alone had a high
328 concentration of silver, 67.7 ± 2.1 and 1.36 ± 0.025 mg/L respectively. Where the coatings
329 contained Ag NPs, total Ag (form unknown) was readily measured in the broth (Figure
330 4A). The broth exposed to both TiO_2-Ag7 and TiO_2-Ag7–HA discs had 2.08 ± 0.2 and
331 0.50 ± 0.1 mg/L of total Ag respectively (significantly less total Ag from TiO_2-Ag7–HA
332 (Kruskal-Wallis, $p < 0.05$; $n = 6$). Thus the coating with HA impeded the release of the
333 majority of the silver from the coatings in the presence of the broth.
334

335 ***Cell morphology and survival***

336 Specimens from the controls and treatments were examined for abundance and
337 morphology of the bacteria by electron microscopy at the end of the experiment (Figure
338 5). As expected the bacteria cultured directly on the plastic wells (control) survived and
339 grew on the whole surface (Figure 5A). The bacteria also grew on the TiO_2-NTs (Figure
340 5B), but were sparse or absent on all the Ag-containing materials (Figures 5C-F). The

electron microscopy observations were consistent with by the proportions of live bacteria detected using the L7012 LIVE/DEAD® Backlight™ Kit after a 24 h of exposure to the composite materials or the controls (Figure 6). The percentage of live bacteria was high in the broth (72.5 ± 2.9%) and on the surface of the plastic well (100.9 ± 2.6%), as expected. The control cells were the most metabolically active compared to all other treatments (Kruskal Wallis, $p < 0.05$, $n = 6$) as confirmed by the lactate production assay (Figures 6C-D).

Slightly few bacteria grew on the TiO_2-NTs, but with >80% alive on the surface this material was not biocidal. In contrast, the bacteria exposed to silver controls ($AgNO_3$ or dispersions of Ag NP) were dead (< 1% live bacteria) and with negligible lactate production (0.2 mM or much less, Figure 6). $AgNO_3$ and Ag NPs were equally effective biocides (not statistically different from each other, Figure 6). Both TiO_2-Ag7 and TiO_2-Ag7–HA coatings had a significantly lower percentage of live to dead cells (6.74 ± 0.98% and 1.78 ± 0.29% respectively) as compared to the control or TiO_2-NTs. The TiO_2-Ag7 was as effective as $AgNO_3$ or dispersions of Ag NPs at killing bacteria with only 3.4 ± 0.3% live on the former and negligible lactate production (Figures 6A and C). Notably, with the addition of nHA, the TiO_2-Ag7–HA coating still retained most of its biocidal properties with 13.9 ± 1.0% of live cells attached to its surface and only 1.07 ± 0.03 mM of lactate production (Figures 6A and C).

Discussion

Improved fabrication and Ag release from the composite coating

In this study, TiO_2-NTs were successfully decorated with a uniform distribution of individual Ag NPs on the surface (Figure 1C). This is a marked improvement on our previous attempts to reduce silver ions to Ag NPs on the surface of TiO_2-NTs using the

biocompatible reducing agent, δ-gluconolactone (Gunputh *et al.*, 2018), where the distribution of the nanoparticles was not uniform and showed micron and nano-sized clusters of the particles. Furthermore, in the present study the as formed TiO_2-NTs were initially treated at 350℃ to increase their chemical stability (Zazpe *et al.*, 2017) followed by an alkaline treatment in 2 mol/L NaOH which made the nanotube more receptive to silver ammonia solution. When the TiO_2-NTs react with NaOH, sodium titanate crystals are formed on the nanotubes (Tsai and Teng, 2006) as per Equation (1):

$$2TiO_2 + 2NaOH \rightarrow Na_2Ti_2O_5.H_2O \quad (1)$$

When exposed to silver ammonia solution, the Na^+ is substitued by the silver ammonia complex as per Equation (2) (Gunputh *et al.*, 2018).

$$Na_2Ti_2O_5.H_2O + 2[Ag(NH_3)_2]^+ \rightarrow [Ag(NH_3)_2]_2 - Ti_2O_5.H_2O \quad (2)$$

The latter attachment of the silver ammonia to titanate is stronger than the bond in the TiO_2-$[Ag(NH_3)_2]^+$ complex (Gunputh *et al.*, 2018). Hence, the exposure to δ-gluconolatone reduced the silver comples to silver nanoparticles still attached to the nanotubes as per Equations (3) below.

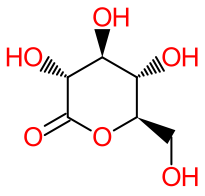

$$+ [Ag(NH_3)_2]_2\ Ti_2O_5.H_2O \rightarrow$$

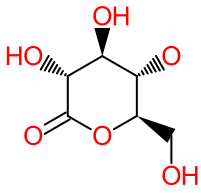

$$+ 2Ag^0\ TiO_2 + 2H_2O + 4NH_3 + H^+ \quad (3)$$

In the presence of δ-gluconolactone, the silver ammonia, while still being attached to the nanotubes, is reduced to Ag NPs. Hence, the decoration is achieved, and by modifying

386 the incubation time the clustering and size of the Ag NPs can be controlled (Gunputh *et*
387 *al.*, 2018). In the present study this was optimised, with the TiO_2-Ag7, achieving the
388 desired decoration (Figure 1C). Further details on the stability of the TiO_2-NTs such as
389 the current density, porosity, pH effects, and Gibbs free energy can be found elsewhere
390 (Danookdharree *et al.*, 2015). The absence of high Ag concentrations in the broth at the
391 end of the experiment also suggests the TiO_2-NTs with their Ag NP decoration was
392 remaining attached to the Ti alloy. The visible presence of Ag NPs on the materials
393 (Figure 1) argues that the Ag is remaining in the reduced form, Ag^0, as expected from x-
394 ray photoelectron spectroscopy (XPS) studies of Ag NPs grown on TiO_2 materials
395 (Kamaraj *et al.*, 2015). Also, the low µg/L releases of Ag by dissolution, suggests very
396 little of the Ag is oxidising (i.e., as assumed soluble Ag^+), and in any event it will
397 spontaneously form sparingly soluble AgCl complexes in the media (Besinis *et al.*,
398 2014a), not silver oxides.

399 For biocidal properties, it is desirable to have a slow release of Ag from the surface
400 of the material. This was achieved with the Ag NPs alone decorated on TiO_2-NTs,
401 releasing µg/L amounts of total Ag into the surrounding biological media (Figures 3 and
402 4). However, the osteoblasts critical to the healing of bone show toxicity and lose around
403 75% of their vital alkaline phosphatase activity when in direct contact with Ag NPs on
404 TiO_2-NTs (Zhao *et al.*, 2011). So, our approach was to include a top coat of nHA, which
405 still allowed some release of dissolved Ag in dialysis experiments with SBF (Figure 3)
406 and into the broth during exposure to *S. aureus* (Figure 4).

407

408 ***Antibacterial properties***

409 In the present study, as expected, the TiO_2-Ag7 coating was biocidal with almost no live
410 bacteria attached to the surface or remaining suspended in the broth (Figures 5 and 6).

411 Indeed, the TiO_2-Ag7 coating was as potent as $AgNO_3$ solution or dispersions of free Ag
412 NPs (Figures 5 and 6). The biocidal properties in this circumstance could arise either from
413 direct contact toxicity of the Ag NPs on the cell walls of the bacteria, or from any
414 dissolved Ag released (Reidy *et al.*, 2013). It is also theoretically possible for UV light
415 stimulation to catalyse the oxidation of some Ag^0 with TiO_2 to form reactive oxygen
416 species that subsequently kill bacteria (Hajjaji *et al.*, 2018), although this is not relevant
417 to the conditions here. Regardless of mechanisms, there are few reports of the MIC values
418 for Ag NPs suspensions with *S. aureus*. Yuan *et al*. (2017) reported an MIC of 2 µg/mL
419 for a multi-drug resistant stain of *S. aureus.* Similarly for methicillin-resistant *S. aureus*
420 (MRSA), Paredes *et al*. (2014) reported MIC values of around 0.25 µg/mL for Ag NPs.
421 Although neither of these latter studies included silver salt controls or particle dissolution
422 measurements, it suggests that low mg/L concentrations of Ag NPs are biocidal, as
423 observed here (Figures 5 and 6). Dissolved silver is arguably more toxic and as little as
424 50 µg/L can completely kill *S. aureus* in 24 h in physiological saline (Jung *et al.*, 2008).
425 In the present study, dissolution of 2-3 µg/L of dissolved Ag was demonstrated in the
426 dialysis experiments with TiO_2-Ag7 (Figure 3), and this material showed no appreciable
427 microbial biofilm (Figure 5). This magnitude of apparent dissolved Ag release is also far
428 below the acute toxicity values for mammalian cells. For example, fibroblasts have an
429 EC50 of 1.7 mg/L for $AgNO_3$ and between 17-35 mg/L for Ag NPs depending on particle
430 size (Ivask *et al.*, 2014). Bone cement loaded with up to 1% w/v as Ag NPs also has no
431 appreciable toxicity to osteoblasts *in vitro* (Alt *et al.*, 2004). Thus the silver release is
432 biocidal, but not likely to be toxic to the surrounding human tissue.
433 The presence of a nHA top coat did not hinder the antibacterial properties of the
434 implant material (Figure 5). The nHA formed a consistent layer over the TiO_2-NTs
435 decorated with Ag NPs, but with some cracks in the nHA surface (Figure 2). This has

been observed before with nHA coatings and is likely due to differences in the thermal expansion coefficients of nHA compared to the underlying materials (Besinis *et al*., 2017). The small fissures in the nHA coat serve to enable the controlled release of the underlying silver (e.g., from electroplated titanium alloy, (Besinis *et al.*, 2017) and a similar observation was made here with the TiO_2-Ag7-HA treatment (Figures 3 and 4). Thus overall, the fissures in the nHA top coating are a desirable feature that enable the leaching of some Ag to cause antimicrobial properties towards *S. aureus*, and yet the nHA would also provide a known biocompatible surface for human osteoblasts.

In conclusion, the chemical reduction of silver ammonia using δ-gluconolactone was successfully used to synthesise individual Ag NPs that consistently decorated the surface of TiO_2-NTs. Both TiO_2-Ag7 and TiO_2-Ag7-HA exhibited antibacterial properties, but the latter material with a nHA top coat is more desirable from the viewpoint of biocompatibility with human cells. The next step in the research will be to explore the adherence and differentiation of osteoblasts on the TiO_2-Ag7-HA with a view to demonstrating osseointegration of the implant material with human bone.

Acknowledgements

Technical support from the Schools of Marine Science and Engineering, Biological and Biomedical Sciences, and the Electron Microscopy Centre (EMC) at Plymouth University is gratefully acknowledged.

Disclosure Statement

There are no conflicts of interest.

Funding

UG was supported by a joint PhD studentship from the Faculty of Science and Environment and the Peninsular Schools of Medicine and Dentistry.

References

Alt, V., Bechert, T., Steinrücke, P., Wagener, M., Seidel, P., Dingeldein, E., Domann, E. & Schnettler, R., 2004. An *in vitro* assessment of the antibacterial properties and cytotoxicity of nanoparticulate silver bone cement. *Biomaterials,* 25**,** 4383-4391.

Balani, K., Anderson, R., Laha, T., Andara, M., Tercero, J., Crumpler, E. & Agarwal, A., 2007. Plasma-sprayed carbon nanotube reinforced hydroxyapatite coatings and their interaction with human osteoblasts *in vitro*. *Biomaterials,* 28**,** 618-624.

Besinis, A., De Peralta, T. & Handy, R.D., 2014a. The antibacterial effects of silver, titanium dioxide and silica dioxide nanoparticles compared to the dental disinfectant chlorhexidine on *Streptococcus mutans* using a suite of bioassays. *Nanotoxicology,* 8**,** 1-16.

Besinis, A., De Peralta, T. & Handy, R.D., 2014b. Inhibition of biofilm formation and antibacterial properties of a silver nano-coating on human dentine. *Nanotoxicology,* 8**,** 745-754.

Besinis, A., Hadi, S.D., Le, H.R., Tredwin, C. & Handy, R.D., 2017. Antibacterial activity and biofilm inhibition by surface modified titanium alloy medical implants following application of silver, titanium dioxide and hydroxyapatite nanocoatings. *Nanotoxicology,* 11**,** 327-338.

Brammer, K.S., Frandsen, C.J. & Jin, S., 2012. TiO_2 nanotubes for bone regeneration. *Trends in Biotechnology,* 30**,** 315-22.

Chernozem, R.V., Surmeneva, M.A., Krause, B., Baumbach, T., Ignatov, V.P., Prymak, O., Loza, K., Epple, M., Ennen-Roth, F. & Wittmar, A., 2019. Functionalization of titania nanotubes with electrophoretically deposited silver and calcium phosphate nanoparticles: structure, composition and antibacterial assay. *Materials Science and Engineering: C,* 97**,** 420-430.

Chernozem, R.V., Surmeneva, M.A., Krause, B., Baumbach, T., Ignatov, V.P., Tyurin, A.I., Loza, K., Epple, M. & Surmenev, R.A., 2017. Hybrid biocomposites based on titania nanotubes and a hydroxyapatite coating deposited by RF-magnetron sputtering: Surface topography, structure, and mechanical properties. *Applied Surface Science,* 426**,** 229-237.

Connaughton, A., Childs, A., Dylewski, S. & Sabesan, V.J., 2014. Biofilm disrupting technology for orthopedic implants: what's on the horizon? *Frontiers in Medicine (Lausanne),* 1**,** 22.

Danookdharree, U., Le, H. & Tredwin, C., 2015. The effect of initial etching sites on the morphology of TiO_2 nanotubes on Ti-6Al-4V alloy. *Journal of the Electrochemical Society,* 162**,** E213-E222.

Descamps, S., Awitor, K.O., Raspal, V., Johnson, M.B., Bokalawela, R.S.P., Larson, P.R. & Doiron, C.F., 2013. Mechanical properties of nanotextured titanium orthopedic screws for clinical applications. *Journal of Medical Devices,* 7**,** 0210051-0210055.

Gao, A., Hang, R., Huang, X., Zhao, L., Zhang, X., Wang, L., Tang, B., Ma, S. & Chu, P.K., 2014. The effects of titania nanotubes with embedded silver oxide nanoparticles on bacteria and osteoblasts. *Biomaterials,* 35**,** 4223-35.

Gunputh, U.F., Le, H., Handy, R.D. & Tredwin, C., 2018. Anodised TiO_2 nanotubes as a scaffold for antibacterial silver nanoparticles on titanium implants. *Materials Science and Engineering: C,* 91**,** 638-644.

Ha, S.-W., Jang, H.L., Nam, K.T. & Beck, G.R., 2015. Nano-hydroxyapatite modulates osteoblast lineage commitment by stimulation of DNA methylation and regulation of gene expression. *Biomaterials,* 65**,** 32-42.

Hajjaji, A., Elabidi, M., Trabelsi, K., Assadi, A., Bessais, B. & Rtimi, S., 2018. Bacterial adhesion and inactivation on Ag decorated TiO_2-nanotubes under visible light: Effect of the nanotubes geometry on the photocatalytic activity. *Colloids and Surfaces B: Biointerfaces,* 170**,** 92-98.

Ivask, A., Kurvet, I., Kasemets, K., Blinova, I., Aruoja, V., Suppi, S., Vija, H., Käkinen, A., Titma, T. & Heinlaan, M., 2014. Size-dependent toxicity of silver nanoparticles to bacteria, yeast, algae, crustaceans and mammalian cells *in vitro*. *PloS one,* 9**,** e102108.

Jung, W.K., Koo, H.C., Kim, K.W., Shin, S., Kim, S.H. & Park, Y.H., 2008. Antibacterial activity and mechanism of action of the silver ion in *Staphylococcus aureus* and *Escherichia coli*. *Applied and Environmental Microbiology,* 74**,** 2171-2178.

Kamaraj, K., George, R., Anandkumar, B., Parvathavarthini, N. & Mudali, U.K., 2015. A silver nanoparticle loaded TiO_2 nanoporous layer for visible light induced antimicrobial applications. *Bioelectrochemistry,* 106**,** 290-297.

Kokubo, T., Kushitani, H., Sakka, S., Kitsugi, T. & Yamamuro, T., 1990. Solutions able to reproduce *in vivo* surface-structure changes in bioactive glass-ceramic A-W3. *Journal of Biomedical Materials Research,* 24**,** 721-734.

Meyerink, J.G., Kota, D., Wood, S.T. & Crawford, G.A., 2018. Transparent titanium dioxide nanotubes: Processing, characterization, and application in establishing cellular response mechanisms. *Acta biomaterialia,* 79**,** 364-374.

Moriarty, T.F., Kuehl, R., Coenye, T., Metsemakers, W.-J., Morgenstern, M., Schwarz, E.M., Riool, M., Zaat, S.a.J., Khana, N., Kates, S.L. & Richards, R.G., 2016. Orthopaedic device-related infection: current and future interventions for improved prevention and treatment. *EFORT Open Reviews,* 1**,** 89-99.

Nie, B., Long, T., Ao, H., Zhou, J., Tang, T. & Yue, B., 2017. Covalent immobilization of enoxacin onto titanium implant surfaces for inhibiting multiple bacterial species infection and *in vivo* methicillin-resistant *Staphylococcus aureus* infection prophylaxis. *Antimicrobial Agents and Chemotherapy,* 61, e01766-16.

O'brien, F.J., 2011. Biomaterials & scaffolds for tissue engineering. *Materials Today,* 14**,** 88-95.

Parcharoen, Y., Kajitvichyanukul, P., Sirivisoot, S. & Termsuksawad, P., 2014. Hydroxyapatite electrodeposition on anodized titanium nanotubes for orthopedic applications. *Applied Surface Science,* 311**,** 54-61.

Paredes, D., Ortiz, C. & Torres, R., 2014. Synthesis, characterization, and evaluation of antibacterial effect of Ag nanoparticles against *Escherichia coli* O157:H7 and methicillin-resistant *Staphylococcus aureus* (MRSA). *International Journal of Nanomedicine,* 9**,** 1717-1729.

Ramires, P.A., Romito, A., Cosentino, F. & Milella, E., 2001. The influence of titania/hydroxyapatite composite coatings on in vitro osteoblasts behaviour. *Biomaterials,* 22**,** 1467-1474.

Reidy, B., Haase, A., Luch, A., Dawson, K. & Lynch, I., 2013. Mechanisms of silver nanoparticle release, transformation and toxicity: a critical review of current knowledge and recommendations for future studies and applications. *Materials,* 6**,** 2295.

559 Rodríguez-Cano, A., Pacha-Olivenza, M.-Á., Babiano, R., Cintas, P. & González-
560 Martín, M.-L., 2014. Non-covalent derivatization of aminosilanized titanium
561 alloy implants. *Surface and Coatings Technology,* 245**,** 66-73.
562 Spriano, S., Yamaguchi, S., Baino, F. & Ferraris, S., 2018. A critical review of
563 multifunctional titanium surfaces: New frontiers for improving osseointegration
564 and host response, avoiding bacteria contamination. *Acta Biomaterialia,* 79**,** 1-
565 22.
566 Swank, K. & Dragoo, J.L., 2013. Postarthroscopic infection in the knee following
567 medical or dental procedures. *Case Reports in Orthopedics,* 2013**,** 974017.
568 Tsai, C.-C. & Teng, H., 2006. Structural features of nanotubes synthesized from NaOH
569 treatment on TiO_2 with different post-treatments. *Chemistry of Materials,* 18**,**
570 367-373.
571 Tsikandylakis, G., Berlin, O. & Branemark, R., 2014. Implant survival, adverse events,
572 and bone remodeling of osseointegrated percutaneous implants for transhumeral
573 amputees. *Clinical Orthopaedics and Related Research,* 472**,** 2947-56.
574 Yang, Y., Ao, H.-Y., Yang, S.-B., Wang, Y.-G., Lin, W.-T., Yu, Z.-F. & Tang, T.-T.,
575 2016. *In vivo* evaluation of the anti-infection potential of gentamicin-loaded
576 nanotubes on titania implants. *International Journal of Nanomedicine,* 11**,** 2223-
577 2234.
578 Yuan, Y.-G., Peng, Q.-L. & Gurunathan, S., 2017. Effects of silver nanoparticles on
579 multiple drug-resistant strains of *Staphylococcus aureu*s and *Pseudomonas*
580 *aeruginosa* from mastitis-infected goats: An alternative approach for
581 antimicrobial therapy. *International Journal of Molecular Sciences,* 18**,** 569.
582 Zazpe, R., Prikryl, J., Gärtnerova, V., Nechvilova, K., Benes, L., Strizik, L., Jäger, A.,
583 Bosund, M., Sopha, H. & Macak, J.M., 2017. Atomic layer deposition Al_2O_3
584 coatings significantly improve thermal, chemical, and mechanical stability of
585 anodic TiO_2 nanotube layers. *Langmuir,* 33**,** 3208-3216.
586 Zhang, H., Sun, Y., Tian, A., Xue, X.X., Wang, L., Alquhali, A. & Bai, X., 2013.
587 Improved antibacterial activity and biocompatibility on vancomycin-loaded
588 TiO_2 nanotubes: *in vivo* and *in vitro* studies. *International Journal of*
589 *Nanomedicine,* 8**,** 4379-4389.
590 Zhao, L., Wang, H., Huo, K., Cui, L., Zhang, W., Ni, H., Zhang, Y., Wu, Z. & Chu,
591 P.K., 2011. Antibacterial nano-structured titania coating incorporated with silver
592 nanoparticles. *Biomaterials,* 32**,** 5706-16.

593

594

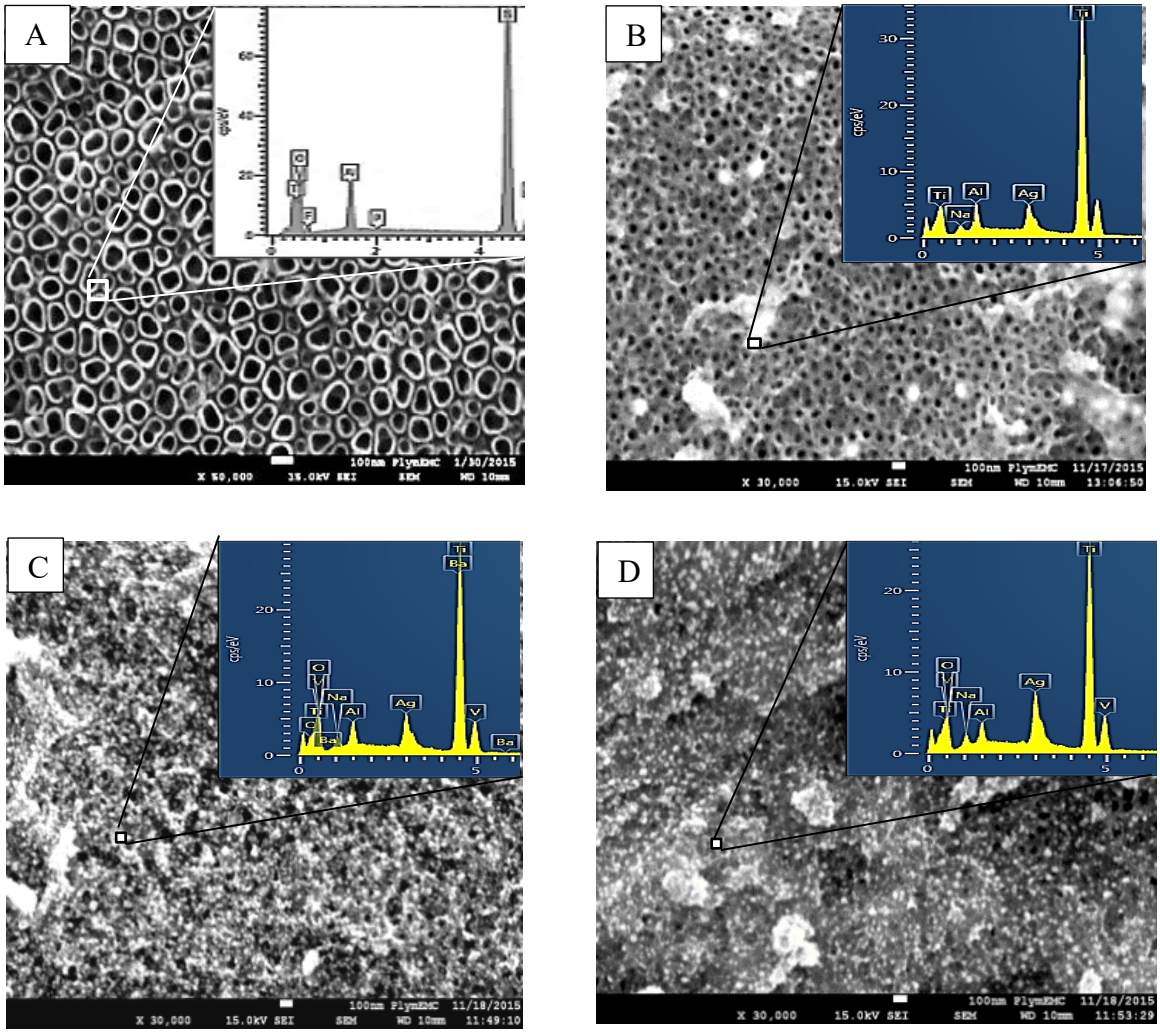

Figure 1: SEM images of Ti-6Al-4V discs coated with (A) TiO_2 nanotubes (×50 000), (B) TiO_2-Ag3 (×30 000), (C) TiO_2-Ag7 (×30 000), (D) TiO_2-Ag10 (×30 000) for incubations of 3, 7 and 10 minutes in silver ammonia solution respectively. The respective EDS analysis are of the Ag NPs formed on the surface represented by white spheres/dots in the images (example images from n = 3 preparations).

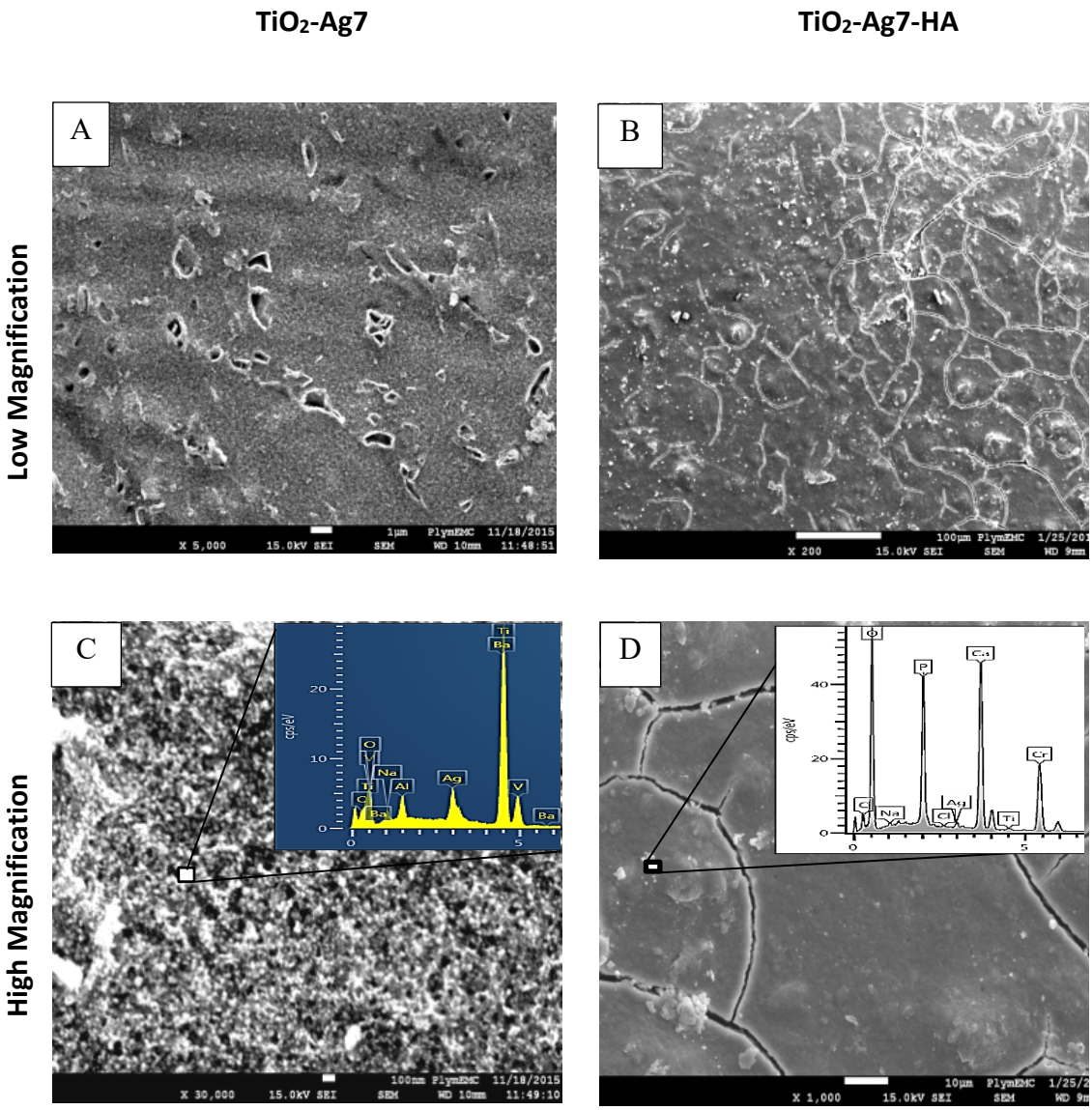

Figure 2: SEM images of (A) TiO_2-Ag7 (×5000) and (B) TiO_2-Ag7-HA (×200) at low magnifications to show coverage of the surface, and their magnified versions in (C, ×30 000) and (D, ×1000) respectively with EDS spectra confirming the expected elemental composition (example images from n = 3 preparations).

600

601

602

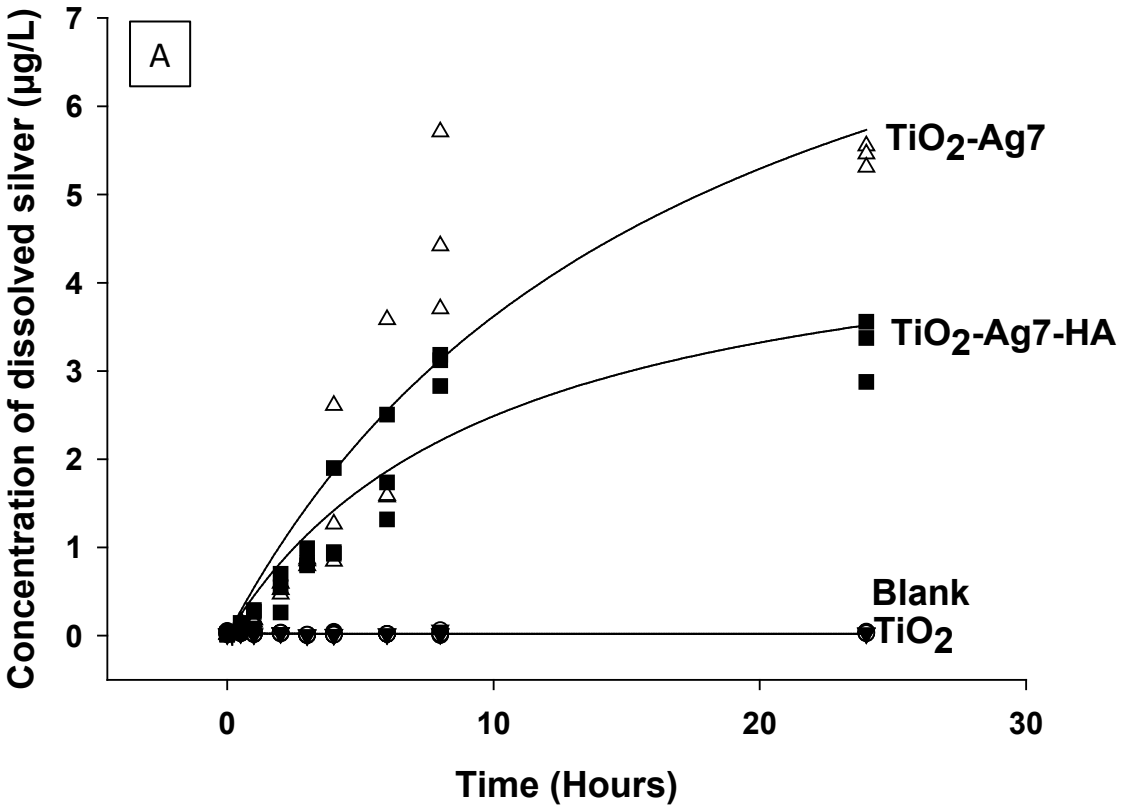
A
Concentration of dissolved silver (µg/L)
7
6
5
4
3
2
1
0
0
10
20
30
Time (Hours)
TiO2-Ag7
TiO2-Ag7-HA
Blank
TiO2

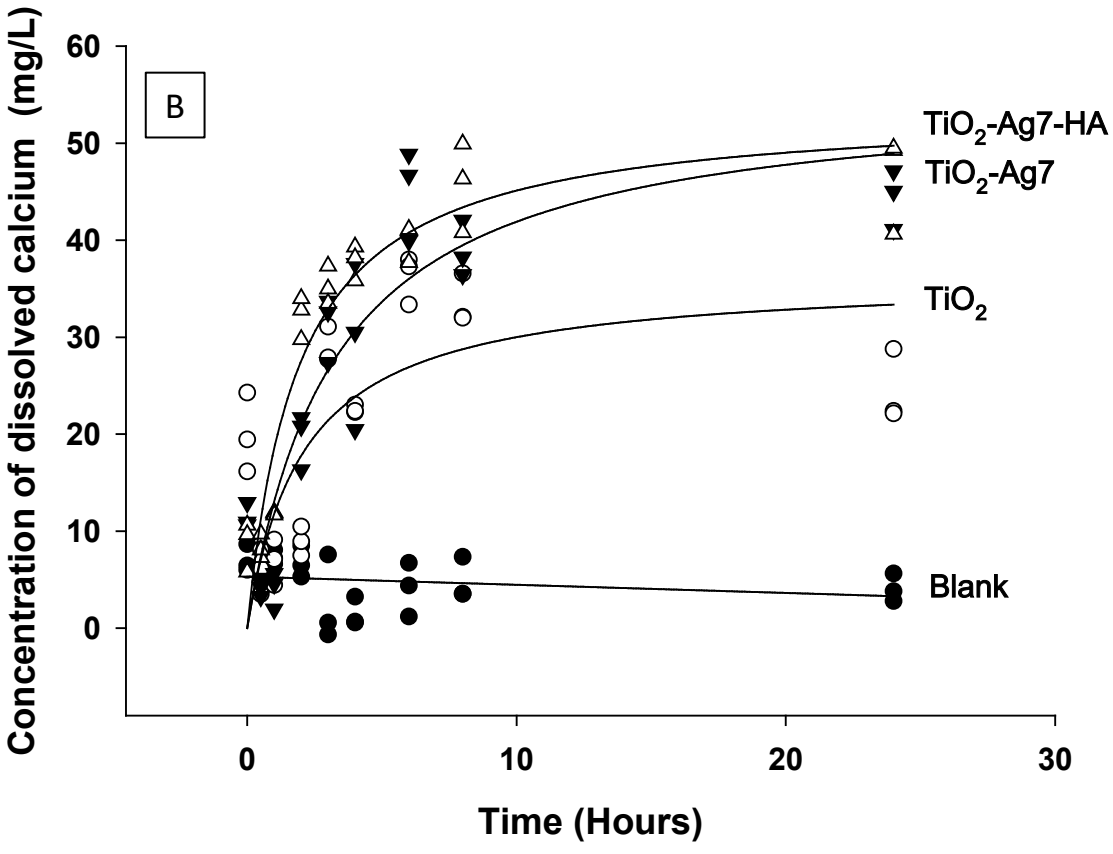
B
Concentration of dissolved calcium (mg/L)
60
50
40
30
20
10
0
0
10
20
30
Time (Hours)
TiO2-Ag7-HA
TiO2-Ag7
TiO2
Blank

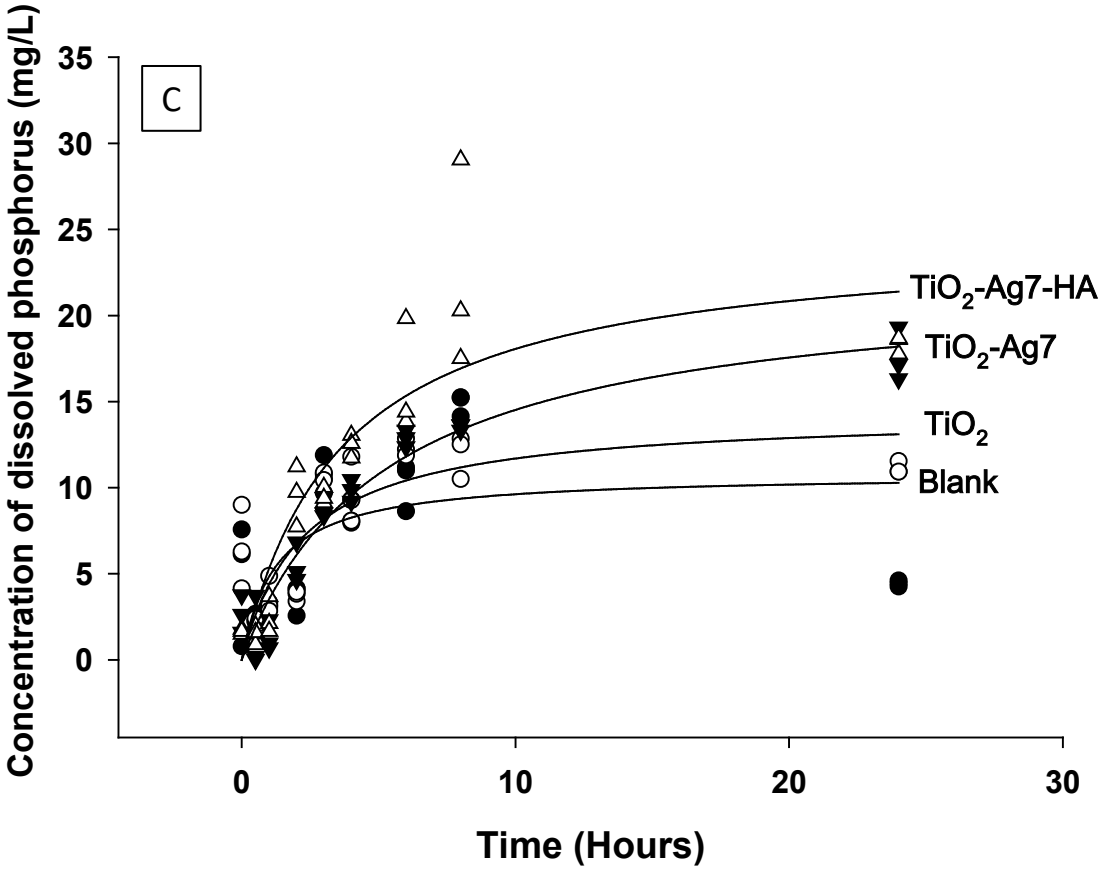

Figure 3: Concentration of (A) total dissolved silver, (B) calcium, and (C) phosphorus measured in simulated body fluid following dialysis of a well without any disc, titanium alloy discs coated with TiO_2 (TiO_2-NTs), TiO_2-Ag7 (TiO_2-NTs decorated with Ag NPs), and TiO_2-Ag7-HA (TiO_2-NTs decorated with Ag NPs, and then a coating of nano hydroxyapatite). Dialysis experiments were performed in triplicate and a rectangular hyperbola function was fitted to the raw data points using Sigmaplot.

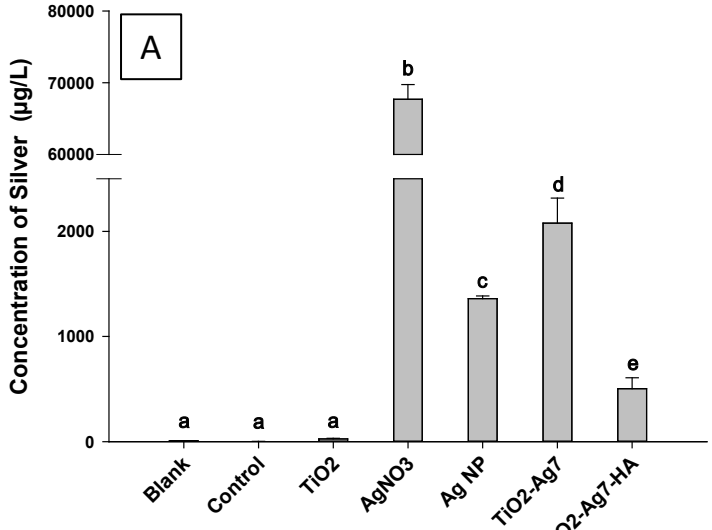
A
Concentration of Silver (µg/L)
80000
70000
60000
2000
1000
0
a
a
a
b
c
d
e
Blank
Control
TiO2
AgNO3
Ag NP
TiO2-Ag7
TiO2-Ag7-HA

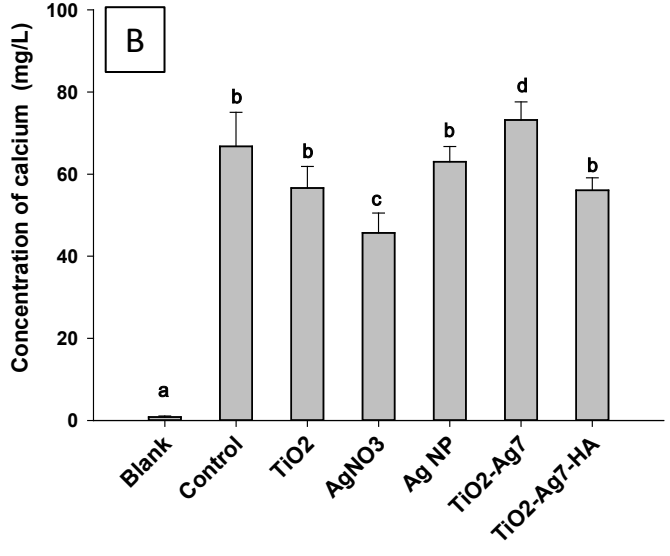
B
Concentration of calcium (mg/L)
100
80
60
40
20
0
a
b
b
c
b
d
b
Blank
Control
TiO2
AgNO3
Ag NP
TiO2-Ag7
TiO2-Ag7-HA

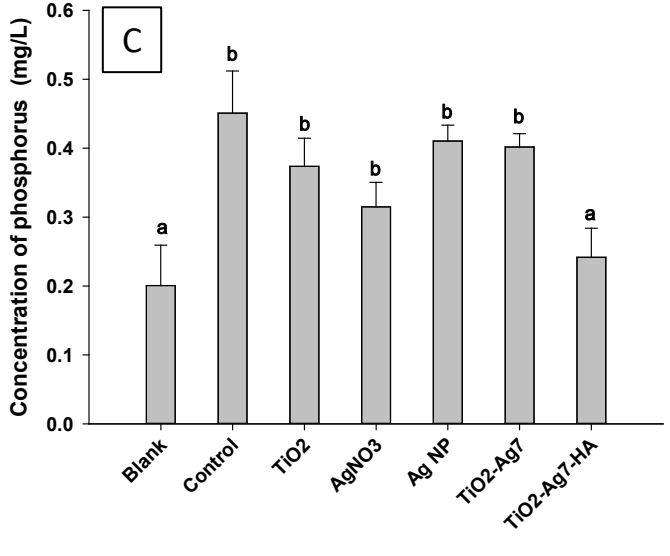
C
Concentration of phosphorus (mg/L)
0.6
0.5
0.4
0.3
0.2
0.1
0.0
a
b
b
b
b
b
a
Blank
Control
TiO2
AgNO3
Ag NP
TiO2-Ag7
TiO2-Ag7-HA

692 Figure 4: Concentration of (A) total silver, (B) calcium, and (C) phosphorus in the exposed broth after overnight growth of *S. aureus* on: Blank
693 (control with no Ti alloy disc, cells grown directly on the plastic culture plate), TiO_2 (TiO_2-NTs), TiO_2-Ag7 (TiO_2-NTs decorated with Ag NPs),
694 and TiO_2-Ag7-HA (TiO_2-NTs decorated with Ag NPs, and then a coating of nano hydroxyapatite). $AgNO_3$ and Ag NPs are silver controls, where
695 the bacteria were grown in broth with silver nitrate solution or a dispersion of Ag NPs (i.e., not as a coating). Values are means ± SEM, n = 6
696 replicates. Different letters indicate a statistically significant difference between treatments ($P < 0.05$, Kruskal-Wallis).

697

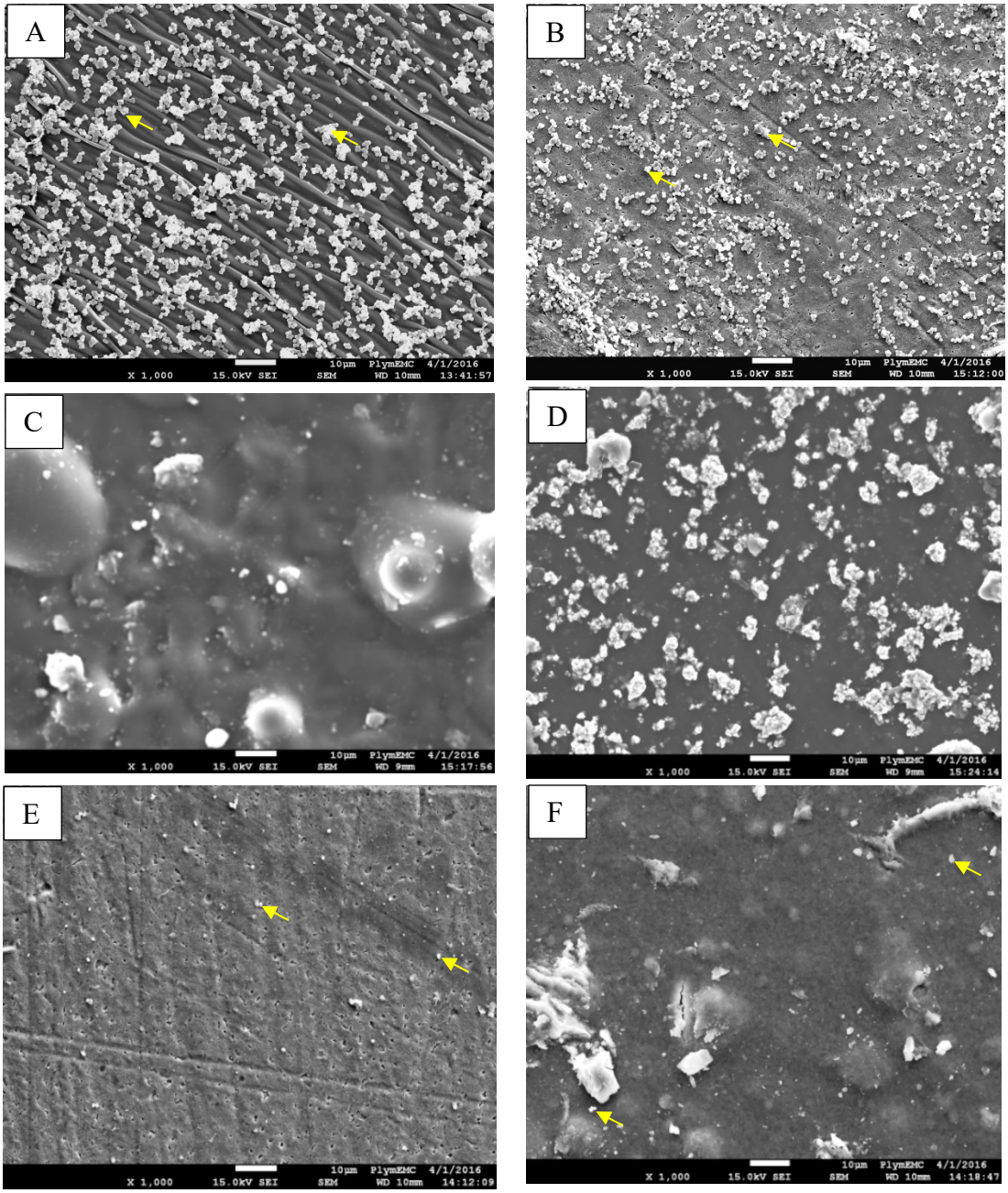

Figure 5: SEM images of attached *S. aureus* (white spherical structures as shown by arrows) after overnight culture in 24-well microplates: (A) Blank (control with no Ti alloy disc, cells grown directly on the plastic culture plate), (B) Ti alloy with TiO_2 nanotubes on the surface (TiO_2-NTs), (C) $AgNO_3$ solution, (D) Ag NPs in suspension, (E) TiO_2-NTs decorated with Ag NPs (TiO_2-Ag7), and (F) TiO_2-NTs decorated with Ag NPs, and then a coating of nano hydroxyapatite (TiO_2-Ag7-HA). Note, the $AgNO_3$ and Ag NPs in suspension are silver controls, where the bacteria were grown with the substances added to the broth (i.e., not as a coating).

698

699

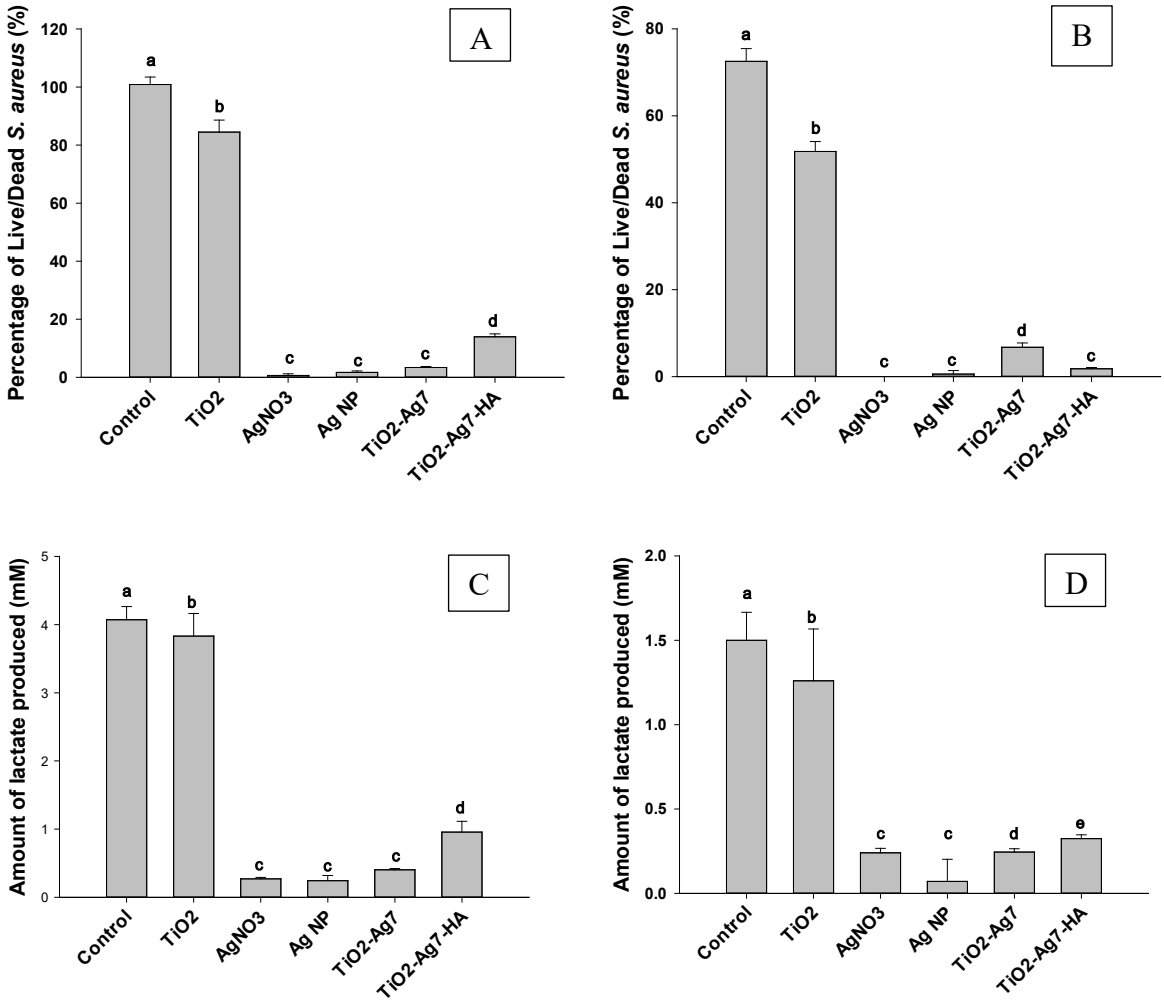

700

701 Figure 6: The proportion of live to dead *S. aureus* (panels A and B) and lactate production
702 (panels C and D) by the organism after 24 h when attached to the surface of the materials
703 (left hand panels), or remaining suspended in the broth (right hand panels). Blank (control
704 with no Ti alloy disc, cells grown directly on the plastic culture plate), TiO_2 (TiO_2-NTs),
705 TiO_2-Ag7 (TiO_2-NTs decorated with Ag NPs), and TiO_2-Ag7-HA (TiO_2-NTs decorated
706 with Ag NPs, and then a coating of nano hydroxyapatite). $AgNO_3$ and Ag NPs are silver
707 controls, where the bacteria were grown in broth with silver nitrate solution or a
708 dispersion of Ag NPs (i.e., not as a coating). Values are means ± SEM, n = 6 replicates.
709 Different letters indicate a statistically significant difference between treatments ($P <$
710 0.05, Kruskal-Wallis).